CrystEngComm

Cite this: *CrystEngComm*, 2012, **14**, 1205

www.rsc.org/crystengcomm

COMMUNICATION

Enhanced photoluminescence of single crystalline ZnO nanotubes in $ZnAl_2O_4$ shell†

Hyun Gil Cha,‡[a] Dong In Kang,‡[a] Tae Ha Kwon*[b] and Young Soo Kang*[a]

Received 31st August 2011, Accepted 8th December 2011
DOI: 10.1039/c2ce06118j

Epitaxial growth of ZnO/$ZnAl_2O_4$ (core/shell) nanotubes from Al_2O_3 coated ZnO nanorods were synthesized using a three-step reaction. In the first step we synthesized ZnO nanorod on Si(100) wafers using chemical vapor deposition, followed by Al_2O_3 deposition on synthesized ZnO nanorod with the help of atomic-layer deposition. Finally in the last step, the resultant sample (*i.e.* Al_2O_3 deposited ZnO nanorod) was calcined at 500 °C for 1 h. Hexagonally well-faceted ZnO nanorod arrays were aligned to Si(100) wafers without metal-catalyst at 500 °C for 1 h. Thereafter it was transformed to spinel-type $ZnAl_2O_4$ nanotubes, which still have ZnO nanotube as a core, by interfacial solid-state reaction in Al_2O_3 coated ZnO nanorods. XRD and Raman analysis demonstrated that single crystallites of both nanotubes co-exist. The photoluminescence spectra show that ZnO nanorod, Al_2O_3 coated ZnO nanorod, ZnO/$ZnAl_2O_4$ (core/shell) nanotube indicated different luminescence bands with different intensity at He–Cd laser excitation (325 nm line).

The controlled preparation of nanomaterials plays a central role in nanoscience and nanotechnology.[1,2] Without controllability, devices based on these nanomaterials are extravagant hopes in most cases. Controllability mainly consists of three parts: composition, morphology, and structure control. Morphology, composition, and structure together govern the chemical, gas sensors, mechanical, electrical, magnetic, and optical properties of the materials that are used to functionalize the devices.[3–8] Especially, the one-dimensional nanostructures, such as nanorods, nanowires, nanobelts, nanotubes *etc.*, have attracted considerable attention for their exceptional, unique, electronic, electrical, optical, and mechanical properties and their potential uses in both fundamental and practical studies.

For example, one dimensional zinc oxide has been demonstrated to be quite effective in lasing, dye-sensitized solar cells, photonic crystals, field emitters, field effect transistors, photodetectors, and even biodevices because of the biocompatibility. It belongs to the wurtzite family of structures with preferential directions of growth that can be utilized to prepare, in a controlled manner, a variety of high-purity nanostructures. In particular, ZnO have a broad band gap (3.37 eV) and a fairly high exciton binding energy (60 meV), which makes it a good candidate for blue-ultraviolet lasing at room temperature.[9] Zinc aluminate (gahnite, $ZnAl_2O_4$), on the other hand, is widely used as ceramic, electronic and catalytic material in synthesis, dehydrogenation, dehydrocyclization, *etc.* With an even broader band gap of 3.8 eV, it can also be used as a transparent conductor, a dielectric, or for optical materials.[10] It can be synthesized by using conventional ceramic processing techniques at high, sol–gel method, coprecipitation method or alumina impregnating method with following calcination at relatively higher temperatures (800–1000 °C).

In the present study, we investigated the photoluminescence property of single crystallized ZnO/$ZnAl_2O_4$ (core/shell) nanotubes prepared by chemical vapor deposition and atomic layer deposition methods based on interfacial solid–solid reaction (see Fig. 1).

The basic idea for the preparation of ZnO nanotubes in a $ZnAl_2O_4$ shell is attributed to the highly enhanced PL intensity and changed the bands of the emission by the different types of nanostructure, such as rod, core/shell, and tube.

The basic idea for the synthesis of single crystallized ZnO/$ZnAl_2O_4$ core–shell type nanotube is very simple, for the following two reasons.

$$Zn\ (g) + 1/2\ O_2\ (g) \rightarrow ZnO\ (\Delta G_o = -320.5\ kJ\ mol^{-1}) \quad (1)$$

$$ZnO + Al_2O_3 \rightarrow ZnO/Al_2O_3 \quad (2)$$

$$ZnO/Al_2O_3 \rightarrow ZnO/ZnAl_2O_4\ (\Delta G_o = 80–400\ kJ\ mol^{-1}) \quad (3)$$

First, the activation energy of reaction, from solid ZnO and Al_2O_3 interfacial reaction was measured to be about 80–400 kJ mol^{-1}, so the Gibbs free energy change for reaction (3) (the overall of reaction 1 and 2) is estimated to be: −335.7 to −15.7 kJ mol^{-1} according to ref. 11 supposing that the entropy change of the reaction is negligibly small and the activation energy is used for the enthalpy change of the reaction under standard conditions. The estimated values imply that reaction (3) is thermodynamically possible. Second, interfacial

[a]*Korea Center for Artificial Photosynthesis, Department of Chemistry Sogang University #1, Shinsu-dong, Mapo-gu, Seoul, 121-742, South Korea. E-mail: yskang@sognag.ac.kr; Fax: +82-1-701-0967; Tel: +82-1-705-8882*
[b]*Department of Electronic Pukyong National University 599-1 Daeyeong 3-dong, Namgu, Busan, 608-737, South Korea*

† Electronic supplementary information (ESI) available: Experimental details on the synthesis and characterization. Normalized PL spectra of ZnO nanorods, Al_2O_3 coated ZnO nanorods, and ZnO/$ZnAl_2O_4$ nanotubes. See DOI: 10.1039/c2ce06118j

‡ These authors contributed equally.

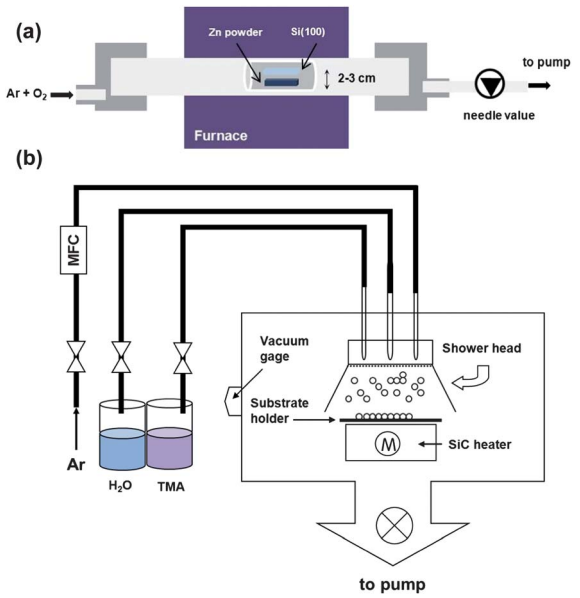

Fig. 1 Schematic illustrations of the setup for ZnO growth and Al_2O_3 coating on the surface of ZnO nanorods. (a) A horizontal CVD system and (b) vertical ALD system which were specially designed for the uniform growth of ZnO nanorods and Al_2O_3 coated ZnO nanorods on Si substrate. The flow rates of Ar and O_2 gases were monitored with MFCs.

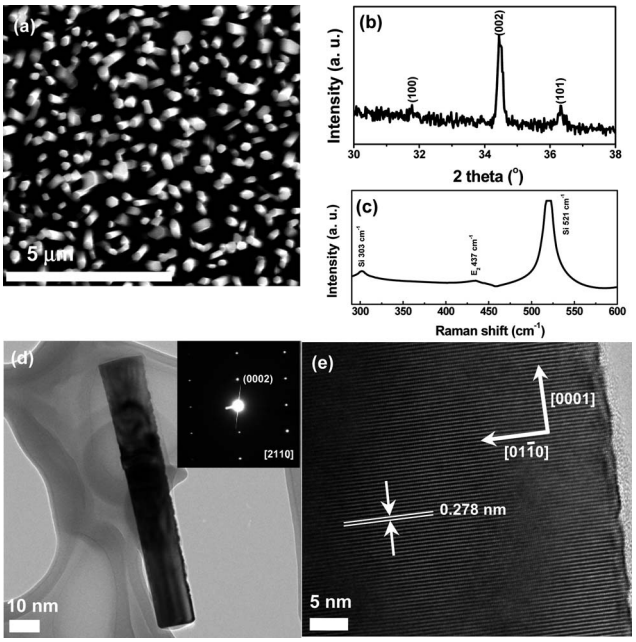

Fig. 2 SEM image (a), XRD pattern (b), Raman spectrum (c), TEM image (d), and HRTEM image (e) of ZnO nanorods on Si(100) substrate at vaporizing temperature of 500 °C for 1 h. (Inset image is SAED pattern of ZnO nanorod.).

reaction[12] and diffusion based on Kirkendall effect between ZnO and Al_2O_3 could be used to grow a crystallized structure out of an amorphous shell, *i.e.* thermally annealed ZnO/$ZnAl_2O_4$ nanotube in an air atmosphere consisted of a single piece that possesses the same lattice structure, lattice orientation, chemical composition.

ZnO nanorods were grown as shown in scanning electron microscopy (SEM) images that show a high density of nanorods are expitaxially aligned to the Si(100) substrate in Fig. 2a. The presence of hexagonally faceted terminal ZnO nanorods implies that the one-dimensional growth of wurtzite ZnO follows the *c*-axial direction.[13] The achievement of epitaxial and aligned ZnO nanowires on Si wafers demonstrates that, during the growth process, stress caused by lattice mismatch can be suppressed at growth temperature and also by stress relaxation effects from nanorods. Since no metal-catalyst of any kind was employed in our synthesis, the growth mechanism of ZnO nanowires cannot be explained using the vapor–liquid–solid (VLS) model.[14] It is reasonable to consider that zinc oxides or sub-oxide clusters deposited on silicon substrates serve as the nucleation center for ZnO nanorods as follows: if the supersaturation is below the value required for the formation of a crystal of some material with euhedral morphology, anisotropic 1D growth in specific crystal directions (which is [0001], in the case of wurtzite ZnO) possibly occur. The crystal structure of the nanorods was examined by XRD. Fig. 2b shows a typical XRD pattern of the ZnO nanowires. The diffraction peaks can be indexed to a hexagonal structure of bulk ZnO with cell constants of $a = 3.24$ and $c = 5.19$ (JCPDS card no. 36-1451).[15] This attribution is also supported by Raman spectroscopy measurement.

The Raman active modes are: Al + $2E_2$ + E1,[16] where the E_2 mode represents the wurtzite structure. As shown in Fig. 2c, the peak 437 cm^{-1} is assigned the ZnO nonpolar optical phonons mode. As we know, the red shift of the Raman peak in the nanomaterials is usually relative to three factors; phonon confinement effect caused by the nanosize of the material, defects, and strains. Three results of Raman measurements imply that the nanorods are of high quality and almost free of defects and strains.

Further structural characterization of the ZnO nanorods was performed using TEM. Fig. 2d shows that an obtained sample is straight with a 103 nm diameter and 950 nm length. Moreover, no additional metal particle appeared on the top or bottom of the rod, implying that a non-VLS approach[2] to the growth of the well-aligned ZnO nanorods was achieved. The SAED pattern (Fig. 2d, inset) reveals that the obtained ZnO nanorods exhibit a single crystal structure with wurtzite type, which is in agreement with XRD and Raman results. A high-resolution TEM image of a ZnO nanorod (Fig. 2d) indicated the lattice spacing of 0.258 nm corresponds to the *d*-spacing of (0002) crystal planes, confirming the XRD analysis that the ZnO nanorods are preferentially oriented in the *c*-axis direction.

The Al_2O_3 coated ZnO nanorods after ALD are shown in Fig. 3. Atomic layer deposition (ALD) is a vapor-phase thin film growth technique allowing atomic-scale thickness and uniformity control. Due to the conformal and slow deposition rate characteristics of ALD, the thickness of the Al_2O_3 coating formed on the surface of ZnO nanorods can be highly uniform and precisely controlled. From SEM images of the ZnO nanorods coated with κ-Al_2O_3 layers in Fig. 3a, we can see that there is no obvious shape and crystal structure difference between ZnO and Al_2O_3 coated ZnO nanorods. However, the contrast of the TEM images and elemental mapping (Zn, Al, and O) reveals a uniform thickness of the κ-Al_2O_3 on the ZnO nanorods at 200 °C shown in Fig. 4a and c. The Al_2O_3 layer has a very uniform thickness of 27.5 nm along the ZnO nanorods. The precise control of the shell thickness is attributed to the sequential and self-limiting ALD process, which avoids any gas-phase reaction in the system and allows the target Al_2O_3 film to grow layer-by-layer around the ZnO nanorod.

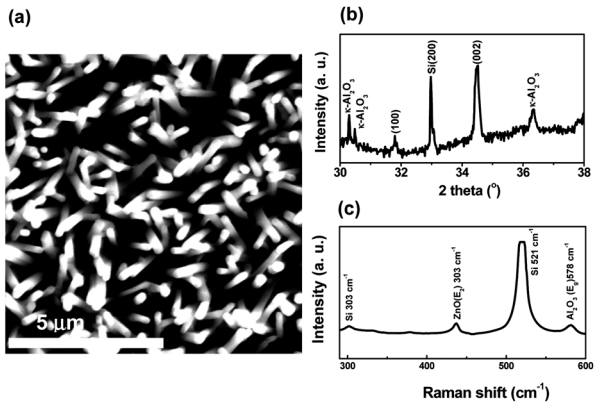

Fig. 3 SEM image (a), XRD pattern (b), and Raman spectrum (c) of Al_2O_3 coated ZnO nanorods on Si(100) substrate at vaporizing temperature of 500 °C for 1 h.

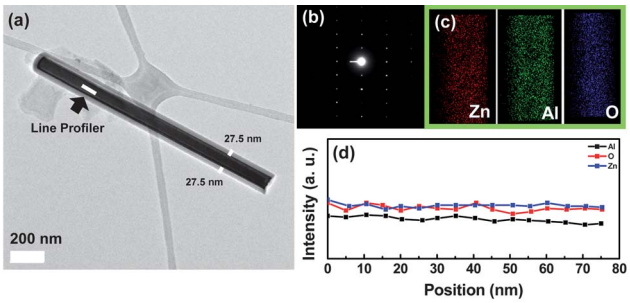

Fig. 4 TEM image (a), SAED pattern (b), elemental mapping images (c), and intensity profile (d) of Zn, Al, and O across of the ZnO/Al_2O_3 nanorods prepared by using ALD 180 cycles. The corresponding SAED pattern obtained from the ZnO/Al_2O_3 nanorod projected along the [2110] axis.

Fig. 3 (b) show the XRD pattern of κ-Al_2O_3 coated ZnO nanorods. With the exception of the Si (100) substrate, XRD data is consistent with hexagonal structure ZnO (JCPDS card no. 36-1451) and κ-Al_2O_3 (JCPDS card no. 88-0107). The intensity of ZnO main peak at 34.50 was relatively deduced after κ-Al_2O_3 coating on ZnO nanorods with respect to that of ZnO nanorods. This attribution is also supported by Raman spectroscopy measurement. Fig. 3c shows the Raman signals from Al_2O_3 coated ZnO nanorods containing ZnO 1-LO and 2-LO modes,[16] in addition to Al_2O_3 signals. Al_2O_3 belongs to the $D_{3d}6$ space group and has two molecular Al_2O_3 groups per unit cell. Peak position of the only two main peaks, 378 and 578 cm^{-1}, in the Raman spectra can be assigned to the alumina gels reported by Assih *et al.*[17] The local composition of the Al_2O_3 coated ZnO nanorod was investigated with TEM-EDS spectra by elemental mapping and line scanning along one nanorod in Fig. 4d. The intensity profile of elements Al, Zn, and O along the nanorod was conducted. The atomic ratio of Zn/Al is about 1.8 : 1.

Fig. 5a shows representative SEM images of the spinel core/shell nanotube after thermal annealing of the Al_2O_3 coated ZnO nanorods at 700 °C for 4 h under an air atmosphere. The shape is not much different compared with Fig. 2a and 3a.

As shown Fig. 5b, XRD pattern demonstrates the formation of a crystalline $ZnAl_2O_4$ phase (JCPDS card no.05-0669)[10] with ZnO and γ-Al_2O_3 on Si(100) substrate. $ZnAl_2O_4$ materials with spinel

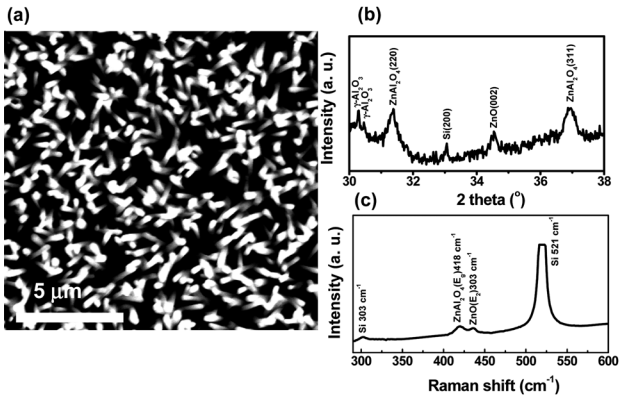

Fig. 5 SEM image (a), XRD pattern (b), and Raman spectrum (c) of annealed Al_2O_3 coated ZnO nanorods on Si(100) substrate at 700 °C for 4 h.

structure belong to the space group O_h^7 with eight formula units in the unit cell. Thirty two oxygen atoms occupy sites with C_{3v} symmetry forming a closely packed cubic lattice with 64 tetrahedral (T_d) and 32 octahedral (D_{3d}) cation sites, only 8 tetrahedral (8A) and 16 octahedral (16B) of them being occupied by cations. $ZnAl_2O_4$ compound under study belong to normal spinels, where all Zn atoms occupy the tetrahedral A sites. A Raman spectrum of annealed ZnO/Al_2O_3 (core/shell) nanorods is given in Fig. 5c. Clearly, the E_g mode at 418 cm^{-1} of spinel phase, $ZnAl_2O_4$,[18] has been measured with the E_2 mode at 437 cm^{-1} of the wurtzite structure corresponding to ZnO.

Most of the core/shell nanotubes are formed as hollow from one end to the other. These nanotubes are freestanding, narrow (84 nm in shell thickness, 68 nm in inner diameter), and highly single crystallized $ZnO/ZnAl_2O_4$ (core/shell) nanotubes in Fig. 6a. The SAED pattern (Fig. 6a, inset) clearly reveals that the tubular structure grown preferentially with the (111) crystal plane of cubic $ZnAl_2O_4$ nanotube out of ZnO nanotube. The intensity profile of elements Al, Zn, O across the $ZnO/ZnAl_2O_4$ (core/shell) nanotube in Fig. 6b presents a ravine-like shape characteristic of completely single crystallized $ZnO/ZnAl_2O_4$ (core/shell) nanotube. For a formed nanotube with a diameter 68 nm, the atomic ratio of elemental Zn/Al/O is about 3.2 : 1 : 4.3 indicating the existence of oxygen deficiencies. Thus, the

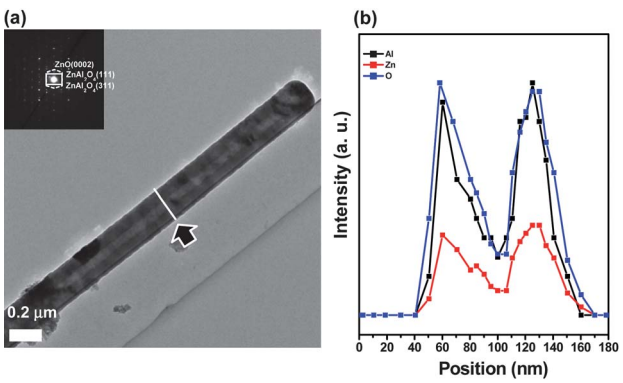

Fig. 6 TEM image (a) and intensity profile (b) of Zn, Al, and O across one tube diameter. (Inset image is SAED pattern of annealed Al_2O_3 coated ZnO nanorod at 700 °C for 4 h).

tube possibly consisted of ZnO and $ZnAl_2O_4$ nanotubes. The results indicate that the single crystal $ZnAl_2O_4$ can be formed between ZnO nanorods and κ-Al_2O_3 layer at 700 °C for 5 h under air.

As compared with Fig. 4, the γ-Al_2O_3 out shell in thermal-annealed Al_2O_3 coated ZnO on Si wafer play an important role in single crystallization, acting as a 'compliant', provide a lower lattice mismatch between ZnO and γ-Al_2O_3.[19] Of importance to our design principle are the requirements that γ-Al_2O_3 coating around the ZnO nanorod during thermal-annealing is uniform and the interface between γ-Al_2O_3 and ZnO is defect-free. Thus, we supposed that ZnO nanotubes in $ZnAl_2O_4$ shell transformed from ZnO/Al_2O_3 (core/shell) nanorods by thermal-annealing in an air atmosphere.

The optical properties of single crystallized ZnO/$ZnAl_2O_4$ (core/shell) nanotubes from ZnO/Al_2O_3 (core/shell) nanorods by thermal annealing at air in atmosphere were examined by photoluminescence (PL) measurements at room temperature. Fig. 7a shows the typical PL spectrum of ZnO nanorods. Two bands have appeared a strong, sharp, and dominating band at 3.28 eV in the UV region and a weak and suppressed band at 2.14 eV nm in the visible regions have been observed.[20] It is believed that the high crystalline quality ZnO shows a dominant UV emission with a week green emission. In Fig. 7b, there is a new emission band (1.91 eV) of ZnO/Al_2O_3 (core/shell) nanorods. It is possibly interpreted as the Al–O–Zn bonds on the surface of ZnO nanorods and Al_2O_3 shell gives red emission band. After thermal annealing ZnO/Al_2O_3 nanorods transformed to ZnO/$ZnAl_2O_4$ core/shell nanotubes as shown in Fig. 7c. Comparison of curves a and c indicates that the ZnO nanotube located inside of $ZnAl_2O_4$ nanotube, *i.e.* core/shell structure, cause a significant photoluminescence enhancement. The maximum intensity of ZnO/$ZnAl_2O_4$ nanotube at ~3.26 eV, attributed to the radiation recombination of free exciton transition from the conduction band to the valence band, indicated 15 times higher than ZnO nanorods. From this result, we expect that embedding ZnO nanotube into $ZnAl_2O_4$ shell induces a change of a local electronic structure of the ZnO nanotube surface due to a different dielectric constant of the surrounding materials[21] and ZnO nanotubes have larger surface area compared with ZnO nanorods.[22] The $ZnAl_2O_4$ shell around the ZnO core surface acts as a dielectric material and screens the charge carriers on the surface states, thus lowering energy separation between the Fermi level and the conduction band at the surface of ZnO. It results in a stronger overlap of the wavefunctions of electron and hole in the surface of ZnO and hence in a higher density of near-surface excitons. Also the walls of ZnO/$ZnAl_2O_3$ nanotube have resonant cavity. It may cause strong intensification in the spontaneous emission by whispering gallery mode resonances.[23] An increased density of excitons and resonant cavity from ZnO/$ZnAl_2O_4$ nanotubes leads to 15 times higher PL intensity at 3.26 eV than ZnO nanorod.

The stronger intensity of the green luminescence (2.14–2.43 eV) in ZnO/$ZnAl_2O_4$ nanotube was appeared because of more singly ionized oxygen vacancies, zinc interstitials, common impurities, and defects in the interface between ZnO and $ZnAl_2O_4$.[24] Therefore, the ZnO/$ZnAl_2O_4$ nanotubes exhibited better performance in excitation emission than those of ZnO nanorods and ZnO/Al_2O_3 (core/sell) nanorods. Nevertheless, further investigations are needed to verify the physical mechanism underlying.

In conclusion, we have explored PL property of a new structure, single crystallized ZnO nanotube phosphor in $ZnAl_2O_4$ shell, which comprises vertically aligned ZnO nanorods on Si (100) substrate. The results reveal that single crystallized ZnO/$ZnAl_2O_4$ nanotubes were formed at core/shell interface reaction due to the migration of ZnO based on surface diffusion effect. PL experiment indicated that hollow shaped ZnO nanotubes inside of $ZnAl_2O_4$ have 15 times higher than ZnO nanorods at ~3.26 eV and stronger the intensity of the green luminescence (2.14–2.43 eV) due to porosity, large surface area, high dielectric constant of the surrounding material, and more singly ionized oxygen vacancies at the interface between ZnO and $ZnAl_2O_4$. The prepared ZnO/$ZnAl_2O_4$ (core/shell) nanotubes can have potential application in catalysis, photonics, photoelectronics, piezoelectrics, lasers, dye-sensitized solar cells, information storage, and other fields, even more study needed to understand the physical mechanism. The approach used here may be implemented to prepare other useful solid inorganic materials.

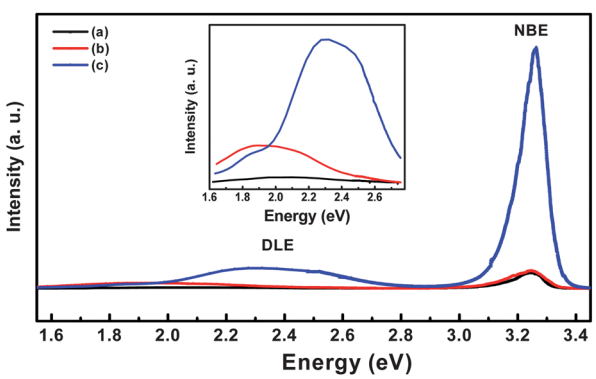

Fig. 7 Room temperature PL spectra of ZnO nanorods (a), Al_2O_3 coated ZnO nanorods (b), and single crystallized ZnO/$ZnAl_2O_4$ nanotubes (c) by using excitation wavelength at 325 nm (He–Cd laser).

Acknowledgements

This work was supported by the Korea Center for Artificial Photosynthesis (KCAP) located in Sogang University funded by the Ministry of Education, Science, and Technology (MEST) through the National Research Foundation of Korea (NRF-2009-C1AAA001-2009-0093879). Dr Kwon was supported by the Pukyong National University Research Abroad Fund in 2008 (ps-2008-034).

Notes and references

1 V. F. Puntes, K. M. Krishnan and A. P. Alivisatos, *Science*, 2001, **291**, 2115.
2 X. F. Duan, Y. Huang, Y. Cui, J. F. Wang and C. M. Lieber, *Nature*, 2001, **409**, 66.
3 S. Cuenot, C. Frétigny, S. D. Champagne and B. Nysten, *Phys. Rev. B: Condens. Matter Mater. Phys.*, 2004, **69**, 165410.
4 Y. W. Jun, S. M. Lee, N. J. Kang and J. Cheon, *J. Am. Chem. Soc.*, 2001, **123**, 5150.
5 C. T. Black, C. B. Murray, R. L. Sandstrom and S. Sun, *Science*, 2000, **290**, 1131.
6 R. Yan, D. Gargas and P. Yang, *Nat. Photonics*, 2009, **3**, 569.
7 K. Seo, N. Bagkar, S. I. Kim, J. In, H. Yoon, Y. Jo and B. Kim, *Nano Lett.*, 2010, **10**, 3643.
8 H. G. Cha, J. Song, H. S. Kim, W. Shin, K. B. Yoon and Y. S. Kang, *Chem. Commun.*, 2011, **47**, 2441.
9 K. A. Dick, K. Deppert, M. W. Larsson, T. Mårtensson, W. Seifert, L. R. Wallenberg and L. Samuelson, *Nat. Mater.*, 2004, **3**, 380.

10 (*a*) Y. Yang, D. S. Kim, R. Scholz, M. Knez, S. M. Lee, U. Gösele and M. Zacharias, *Chem. Mater.*, 2008, **20**, 3487; (*b*) Y. Wang, Q. Liao, H. Lei, X. Zhang, X. Ai, J. Zhang and K. Wu, *Adv. Mater.*, 2006, **18**, 943.
11 H. Okada, H. Kawakami, M. Hashiba, E. Miura, Y. Nurishi and T. Hibino, *J. Am. Ceram. Soc.*, 1985, **68**, 58.
12 Y. Lin, S. Zhou, S. W. Sheehan and D. Wang, *J. Am. Chem. Soc.*, 2011, **133**, 2398.
13 C. Geng, Y. Jiang, Y. Yao, X. Meng, J. A. Zapien, C. S. Lee, Y. Lifshitz and S. T. Lee, *Adv. Funct. Mater.*, 2004, **14**, 589.
14 Y. Qiu, M. Yang, H. Fan, Y. Zuo, Y. Shao, Y. Xu, X. Yang and S. Yang, *CrystEngComm*, 2011, **13**, 1843.
15 J. J. Wu and S. C. Liu, *Adv. Mater.*, 2002, **14**, 215.
16 T. C. Damen, S. P. S. Porto and B. Tell, *Phys. Rev.*, 1966, **142**, 570.
17 T. Assih, A. Ayral, M. Abenoza and J. Phalippou, *J. Mater. Sci.*, 1988, **23**, 3326.
18 E. Zouboulis, D. Renusch and M. Grimsditch, *Appl. Phys. Lett.*, 1998, **72**, 1.
19 A. Chopelas and A. Hofmester, *Phys. Chem. Miner.*, 1991, **18**, 279.
20 W. J. Shen, J. Wang, Q. Y. Wang, Y. Duan and Y. P. Zeng, *J. Phys. D: Appl. Phys.*, 2006, **39**, 269.
21 (*a*) J. P. Richters, T. Voss, L. Wischmeier, I. Rückmann and J. Gutowski, *Appl. Phys. Lett.*, 2008, **92**, 011103; (*b*) P. Reiss, M. Protiere and L. Li, *Small*, 2009, **5**, 154.
22 X. P. Shen, A. H. Yuan, Y. M. Hu, Y. Jiang, Z. Xu and Z. Hu, *Nanotechnology*, 2005, **16**, 2039.
23 (*a*) D. Wang, H. W. Seo, C. C. Tin, M. J. Bozack, J. R. Williams, M. Park and Y. Tzeng, *J. Appl. Phys.*, 2006, **99**, 093112; (*b*) M. Q. Israr, J. R. Sadaf, L. L. Yang, O. Nur, M. Willander, J. Palisaitis and P. O. Å. Persson, *Appl. Phys. Lett.*, 2009, **95**, 073114.
24 K. Vanheusden, W. L. Warren, C. H. Seager, D. K. Tallant, J. A. Voigt and B. E. Gnade, *J. Appl. Phys.*, 1996, **79**, 7983.